Available online at www.sciencedirect.com
ScienceDirect
ELSEVIER
Nuclear Physics A 801 (2008) 83–100
NUCLEAR PHYSICS A
www.elsevier.com/locate/nuclphysa

Lifetimes of intruder states in ^{186}Pb, ^{188}Pb and ^{194}Po

T. Grahn [a,b,*], A. Dewald [c], O. Möller [c,1], R. Julin [a], C.W. Beausang [d,2], S. Christen [c], I.G. Darby [b,3], S. Eeckhaudt [a], P.T. Greenlees [a], A. Görgen [e], K. Helariutta [f], J. Jolie [c], P. Jones [a], S. Juutinen [a], H. Kettunen [a], T. Kröll [g], R. Krücken [g], Y. Le Coz [e], M. Leino [a], A.-P. Leppänen [a,4], P. Maierbeck [g], D.A. Meyer [d,5], B. Melon [c], P. Nieminen [a,6], M. Nyman [a], R.D. Page [b], J. Pakarinen [a,b], P. Petkov [h], P. Rahkila [a], B. Saha [c], M. Sandzelius [a,7], J. Sarén [a], C. Scholey [a], J. Uusitalo [a], M. Bender [i], P.-H. Heenen [j]

[a] *Department of Physics, University of Jyväskylä, PO Box 35, FI-40014 Jyväskylä, Finland*
[b] *Department of Physics, Oliver Lodge Laboratory, University of Liverpool, Liverpool L69 7ZE, UK*
[c] *Institut für Kernphysik, Universität zu Köln, Zülpicher street 77, 50937 Köln, Germany*
[d] *Wright Nuclear Structure Laboratory, Yale University, New Haven, CT 06520, USA*
[e] *CEA-SACLAY, DSM/DAPNIA/SPhN, F-91191 Gif-sur-Yvette cedex, France*
[f] *Laboratory of Radiochemistry, University of Helsinki, PO Box 55, FI-00014 Helsinki, Finland*
[g] *Physik-Department E12, TU München, 85748 Garching, Germany*
[h] *Institute for Nuclear Research and Nuclear Energy, Sofia, Bulgaria*
[i] *Université Bordeaux 1, CNRS/IN2P3, Centre d'Etudes Nucléaires de Bordeaux Gradignan, UMR5797, Chemin du Solarium, BP120, F-33175 Gradignan, France*
[j] *Service de Physique Nucléaire Théorique, Université Libre de Bruxelles, C.P. 229, B-1050 Bruxelles, Belgium*

Received 14 December 2007; received in revised form 7 January 2008; accepted 7 January 2008

Available online 15 January 2008

* Corresponding author at: Department of Physics, Oliver Lodge Laboratory, University of Liverpool, Liverpool L69 7ZE, UK.
E-mail address: tuomas.grahn@liverpool.ac.uk (T. Grahn).
1 Present address: Technical University of Darmstadt, Darmstadt, Germany.
2 Present address: University of Richmond, VA, USA.
3 Present address: University of Tennessee, TN, USA.
4 Present address: STUK, Rovaniemi, Finland.
5 Present address: Rhodes College, Memphis, TN, USA.
6 Present address: Department of Nuclear Physics, ANU, Canberra, ACT 0200, Australia.
7 Present address: Department of Physics, KTH, S-10691 Stockholm, Sweden.

0375-9474/$ – see front matter
doi:10.1016/j.nuclphysa.2008.01.002

Abstract

Lifetimes of prolate intruder states in ^{186}Pb and ^{188}Pb and oblate intruder states in ^{194}Po have been determined through recoil distance Doppler-shift lifetime measurements. Deformation parameters of $|\beta_2| = 0.29(5)$ and $|\beta_2| = 0.17(3)$ have been extracted from experimental B(E2) values for the prolate and the oblate bands, respectively. The present study addresses the phenomenon of shape coexistence typical for the nuclei near $Z = 82$ and $N = 104$, providing information on configuration mixing of intrinsic structures of the nuclei of interest. The results are compared with the available lifetime data and theoretical results for neutron-deficient Po, Pb, Hg and Pt nuclei. Furthermore, new self-consistent mean-field calculations have been carried out for ^{194}Po.

PACS: 21.10.Tg; 23.20.Lv; 27.70.+q; 27.80.+w

Keywords: NUCLEAR REACTIONS ^{106}Pd, ^{108}Pd, ^{114}Cd(^{83}Kr, $3n$), $E = 340$–375 MeV; measured E_γ, γ, $\gamma\gamma$-coin, and lifetimes for intruder states using the recoil distance Doppler-shift method. ^{186,188}Pb, ^{194}Po; deduced B(E2), quadrupole moment, and deformation parameters

1. Introduction

The spectacular phenomenon of shape coexistence observed in nuclei close to the proton drip line near the shell gap at $Z = 82$ and neutron mid-shell at $N = 104$ [1] is an active field of experimental and theoretical studies in nuclear structure physics. The theoretical description of shape coexistence has been driven largely by experimental results and consequently, several theoretical approaches have recently been developed. Competing nuclear shapes are closely associated with the nuclear collective motion and especially quadrupole collectivity at low spin in neutron mid-shell Pb and Po nuclei. Collectivity can be probed in lifetime measurements of nuclear excited states. Since the electromagnetic interaction is well understood, the knowledge of level lifetimes gives direct information about the wave functions of the states of interest.

In even-mass Pb nuclei, deformed structures intrude down in energy close to the spherical ground state when approaching the neutron mid-shell at $N = 104$ [1,2]. In the mid-shell nucleus ^{186}Pb the first two excited states are assigned as deformed 0^+ states. Together with the spherical 0^+ ground state these levels establish a unique shape triplet for which $\pi(2p$–$2h)$ and $\pi(4p$–$4h)$ configurations can be inferred by α-decay studies [3]. In the shell model picture the excitation energies of these configurations are lowered by a residual quadrupole–quadrupole interaction and are predicted to be close to the $\pi(0p$–$0h)$ ground state near the neutron mid-shell [4]. The $\pi(2p$–$2h)$ and $\pi(4p$–$4h)$ excitations can be associated with low-lying oblate and prolate minima, respectively, appearing next to the spherical ground state in the total energy surface calculations based on a deformed mean-field [5,6]. A similar picture is obtained in configuration mixing calculations based on angular momentum projected Hartree–Fock–Bogoliubov (HFB) wave functions [7,8].

Collective yrast bands, similar to those observed in neutron-deficient even-mass Hg and Pt isotopes [1,2], have also been observed in even-mass $^{182–188}$Pb isotopes [9–12]. All these yrast bands have been associated with the prolate minimum. So far, candidates for collective non-yrast bands build on the coexisting oblate structures have been observed only in ^{186}Pb [13] and ^{188}Pb [14].

The extension of spectroscopic studies to $Z = 84$ has revealed intruder structures in neutron-deficient Po isotopes. A sudden drop in level energies is observed in Po isotopes with $N \leqslant 114$,

which is similar to that for the intruding 0_2^+ states observed in α- and β-decay studies of these nuclei. These 0_2^+ states have been associated with $\pi(4p\text{–}2h)$ configurations [15], and on the basis of the Nilsson–Strutinsky calculations they are based on an oblate minimum [5]. Consequently, the observed yrast states in light even-mass Po isotopes down to ^{192}Po are presumed to form oblate bands [2,16]. Based on the observed quadrupole vibrational features of ^{196,198}Po [17], an alternative explanation for the further suppression of level energies in ^{192,194}Po is evolution towards a more collective anharmonic vibrator [18]. In ^{190}Po, a level sequence similar to the prolate bands in $^{182–188}$Pb has been observed [19] to cross the oblate ground state band at low spin. This is in accordance with the earlier Nilsson–Strutinsky calculations [5], which predict the prolate minimum to reach the ground state at ^{188}Po [20,21].

The low spin states in the mid-shell Pb and Po isotopes are predicted to strongly mix oblate and prolate mean-field configurations. Recently, lifetime measurements of excited states [22] as well as spectroscopic studies [14] have established a strong mixing of the 2^+ states in ^{188}Pb. In addition to the simple mixing calculations based on the experimental data, theoretical studies also support the picture of configuration mixing [7,8,23] which will be discussed later in this paper.

Based on the α-decay studies [24,25], mixing of intruder components in ^{192}Po has been deduced. In Ref. [16], by using the observed level patterns in ^{192}Po and ^{194}Po, simple mixing calculations have been carried out. In both of these nuclei, the ground state is predicted to be a strong admixture of intruder and near spherical configurations while the 2^+ yrast state is considered as a pure oblate intruder state. For ^{192}Po and ^{194}Po, configuration mixing calculations have been carried out using the energy level systematics [15]. All these studies indicate an increasing contribution of the deformed structure in the ground state when approaching ^{192}Po, which is also supported by the results obtained with several theoretical models [26].

The degree of deformation has in many cases been deduced experimentally from the kinematic moment of inertia $\mathcal{J}^{(1)}$. This quantity is typically larger for prolate than for oblate bands. However, the deformation deduced from the kinematic moment of inertia depends strongly on the nuclear model used. In a hydrodynamical picture a strong dependence ($\mathcal{J}^{(1)} \propto \beta_2^2$) is expected, while for a rigid rotor the dependence is weak ($\mathcal{J}^{(1)} \propto 1 + 0.3\beta_2$). Therefore, $\mathcal{J}^{(1)}$ cannot be used as a quantitative measure of deformation. However, electromagnetic transition probabilities extracted from measured lifetimes provide a more direct measure of collectivity and allow questions about nuclear shape and mixing to be addressed.

Nuclei in the vicinity of ^{186}Pb can be produced using heavy-ion induced fusion–evaporation reactions which, in turn, enables the use of the Recoil Distance Doppler-Shift (RDDS) method in lifetime measurements. However, due to the low production cross sections of these nuclei a high selectivity in in-beam γ-ray detection is required. Such selectivity can be obtained by using the Recoil-Decay Tagging (RDT) method [27]. In the present work, this method has been employed for the first time in RDDS lifetime measurements of yrast levels in ^{186}Pb and ^{194}Po. In addition, lifetime measurements of the yrast levels in ^{188}Pb up to the 8^+ state were carried out using the recoil-gating method. A summary of the present experimental results has already been published as a Letter [28]. In this paper the experimental results are described in more detail, and new theoretical calculations are presented for ^{194}Po.

2. Experimental details

Excited states of ^{186,188}Pb and ^{194}Po were populated via fusion–evaporation reactions using an ^{83}Kr beam delivered by the K130 cyclotron at the Accelerator Laboratory of the University

of Jyväskylä. Prompt γ rays were detected by the JUROGAM Ge-detector array comprising 43 Ge detectors of EUROGAM Phase I type [29]. The JUROGAM array had 15 detectors at angles suitable for the final lifetime analysis, five at an angle of 158° and ten at an angle of 134° with respect to the beam direction. The standard JUROGAM target chamber was replaced by the Köln plunger device which was especially designed for use with gas-filled recoil separators. The standard stopper foil of the plunger device was replaced by a degrader foil allowing fusion–evaporation residues to recoil into the RITU gas-filled separator [30]. A 50 $\mu g/cm^2$ thick carbon window at the entrance of the target chamber was used to separate the high vacuum of the beam line from 1 mbar He gas inside RITU. Beam intensities between 1 and 3 pnA were used, being limited by the counting rate of the JUROGAM Ge detectors.

The separated recoils were detected at the RITU focal plane in the GREAT spectrometer [31]. The energy loss and timing signals generated by the recoils in flight were recorded with the MultiWire Proportional Counter (MWPC) at the entrance of GREAT. After passing through the MWPC the recoils were implanted into a pair of adjacent Double-sided Silicon Strip Detectors (DSSDs) of GREAT. They were used to provide the position and implantation time information of both the recoiling nuclei as well as their subsequent decay properties. Signals from all the detectors were recorded by employing the Total Data Readout (TDR) data acquisition system, comprising a triggerless system where all channels run independently [32]. In the TDR system, all the signals are time stamped by a global 100 MHz clock. The collected data were reconstructed and analysed off-line using the GRAIN software package [33]. Identification of recoils was made using the energy loss and time-of-flight information provided by the MWPC and DSSDs. Temporal and spatial correlations of a recoil and its subsequent radioactive decay in the DSSDs were performed and singles RDT (^{186}Pb and ^{194}Po) and recoil gated (^{188}Pb) γ-ray spectra were constructed.

The transmission efficiency of RITU for fusion–evaporation residues was reduced due to their small-angle scattering in the degrader foil used in the plunger device. It was necessary to find a compromise between the transmission of RITU and the velocity difference $\Delta v/c$ introduced by the degrader foil. In the first experiment (^{188}Pb) a 2.5 mg/cm^2 thick Au degrader foil reduced the transmission of RITU by a factor of three. Such a heavy material was chosen in order to minimise the number of nuclear reactions generating background events in the JUROGAM detectors. In the later experiments, with low Z materials such as Mg and Al having higher dE/dx values than that of Au, a similar $\Delta v/c$ was obtained with a degrader thickness of 1.0 mg/cm^2. These foils reduced the transmission of RITU only by a factor of two and, as it turned out, did not generate more background radiation than the Au foil.

The intensities of the fully Doppler-shifted (I_s) and degraded (I_d) components of the γ-ray transitions under investigation were determined by fitting the corresponding peak areas. The resulting decay curves ($I_d/(I_s + I_d)$) were analysed according to the principles of the Differential Decay Curve Method (DDCM) [34]. Decay curves constructed from the spectra recorded with the JUROGAM detectors at 158° and 134° were analysed separately. The resulting lifetime of each level is an average of these values.

2.1. Unobserved feeding

In an RDDS measurement based on the use of singles γ-ray spectra one has to deal with unobserved feeding transitions to the level of interest. The time behaviour of unobserved transitions to the level of interest has to be taken into account in the DDCM lifetime analysis in order to extract a reliable value for the lifetime of the level of interest. The intensity of unobserved feeding can

be extracted from the observed relative intensity ratio of feeding and depopulating transitions, i.e., $J_{\text{feed}}/J_{\text{depop}}$ [35].

In the present work, the time behaviour of the unobserved feeding is assumed to be similar to that of the observed direct feeding. This assumption is justified in cases where there is no dominant feeding from a state with a different nuclear structure and the observed feeding times are not particularly long compared to the de-excitation of the level of interest. Experimental tests to validate this hypothesis have been carried out in several cases (e.g., in ^{120}Xe [36] and ^{128}Ba [35,37]) where singles as well as coincidence RDDS measurements were carried out.

With the exception of the 2^+ state in ^{188}Pb all the conditions are fulfilled for the use of the aforementioned feeding time assumption. In addition, if the feeding assumptions are correct, the lifetime values extracted separately in the DDCM analysis for each distances should be similar [34]. In the present work, this argument was used to justify the feeding assumption described above.

2.2. ^{186}Pb

The ^{106}Pd(^{83}Kr, $3n$)^{186}Pb reaction with a beam energy of 357 MeV was used to populate excited states in ^{186}Pb. The lifetimes of the four lowest yrast states in ^{186}Pb have been determined by employing the RDDS method, which was combined for the first time with the RDT technique. Prompt γ-ray spectra tagged with the ^{186}Pb α decay ($t_{1/2} = 4.8$ s, $E_\alpha = 6.38$ MeV) were collected at 11 different target-to-degrader distances ranging from 10 μm to 1600 μm.

A stretched, self-supporting 1.0 mg/cm^2 ^{106}Pd foil was used as a target in the plunger device. The reaction provided an initial recoil velocity of $v/c = 3.8\%$ which yielded the velocity of $v/c = 2.8\%$ with the degrader foils of different materials (2.6 mg/cm^2 Au, 1.0 mg/cm^2 Al and 1.0 mg/cm^2 Mg). The best ^{186}Pb α-particle yield at the RITU focal plane was obtained using the 1.0 mg/cm^2 Mg degrader foil. The estimated cross section for the present reaction was $\sigma \approx 290$ μb. Samples of singles RDT γ-ray spectra are shown in Fig. 1 where, in spite of the low number of events, essentially nonexistent background still enables the peaks of interest to be resolved. The lifetimes of the yrast states in ^{186}Pb were extracted from decay curves measured with the JUROGAM detectors at 158° and 134°. Sample decay curves are shown in Fig. 2 and resulting mean lifetimes τ are summarised in Table 1.

2.3. ^{188}Pb

Due to the relatively long α-decay half-life and low α-decay branching ratio of ^{188}Pb, the RDT method could not be applied in this case. Instead, recoil gated γ-ray spectra were collected at ten target-to-degrader distances ranging from 5 μm to 1600 μm. Yrast states of ^{188}Pb were populated using the ^{108}Pd(^{83}Kr, $3n$)^{188}Pb reaction with a beam energy of 340 MeV. This reaction had an estimated cross section of $\sigma = 1.1$ mb. With an initial recoil velocity of $v/c = 3.8\%$, after a stretched 1.0 mg/cm^2 ^{108}Pd target, the velocity of $v/c = 2.8\%$ was obtained using the 2.5 mg/cm^2 Au degrader foil.

The background in the recoil gated γ-ray spectra (see Fig. 3) was low enough to enable the measurement of lifetimes of the four lowest yrast states in ^{188}Pb. The lifetimes were extracted from the decay curves measured with the JUROGAM detectors at 158° (examples are shown in Fig. 4) and 134°. The similarity of the decay curves for the 2^+ and 4^+ states shows the relatively slow feeding of the 2^+ state. The resulting mean lifetimes τ extracted from the decay curves are given in Table 1.

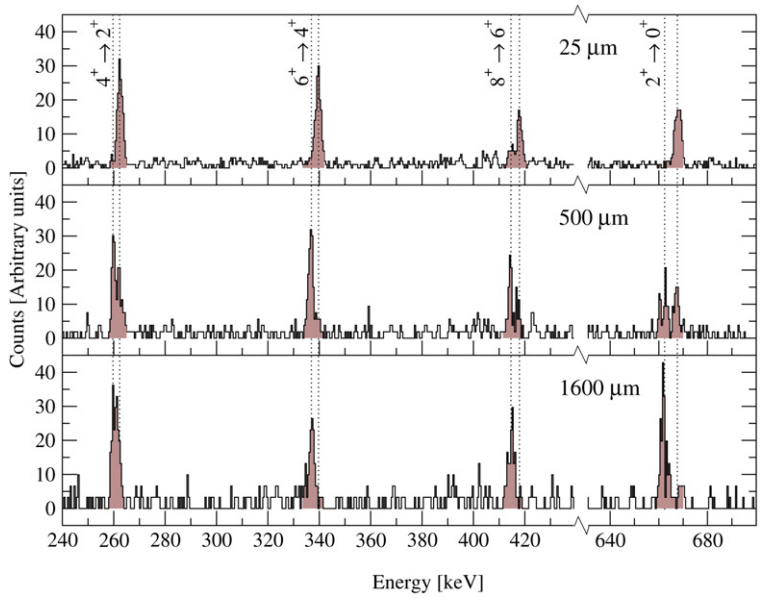

Fig. 1. Singles RDT γ-ray spectra of ^{186}Pb measured at three target-to-degrader distances with five JUROGAM detectors at 158°. Lines indicate the positions of the fully Doppler-shifted and degraded components of the γ rays from the 2^+, 4^+, 6^+ and 8^+ yrast states. Relevant peak areas are shaded to guide the eye.

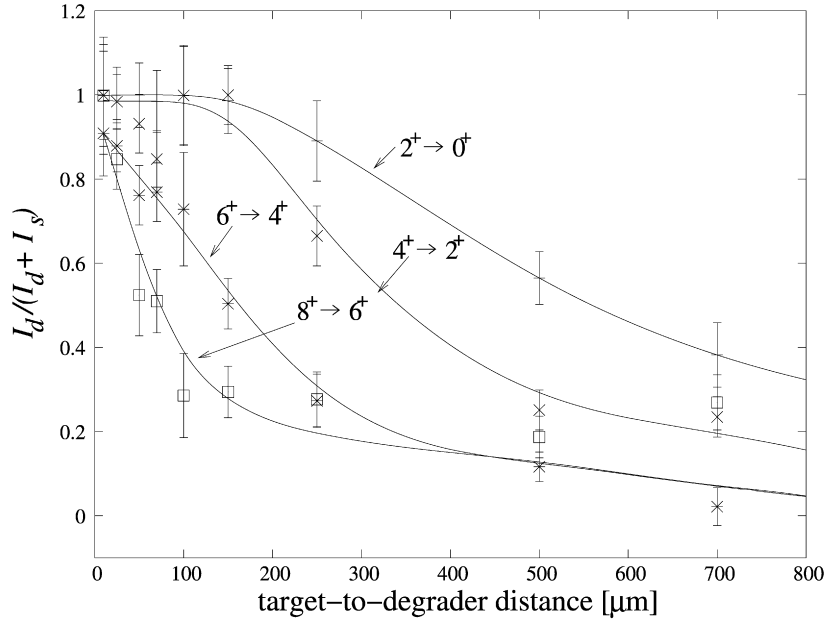

Fig. 2. Decay curves of four lowest yrast states in ^{186}Pb extracted from γ-ray spectra recorded with ten JUROGAM detectors at 134°. The smooth lines are drawn to guide the eye.

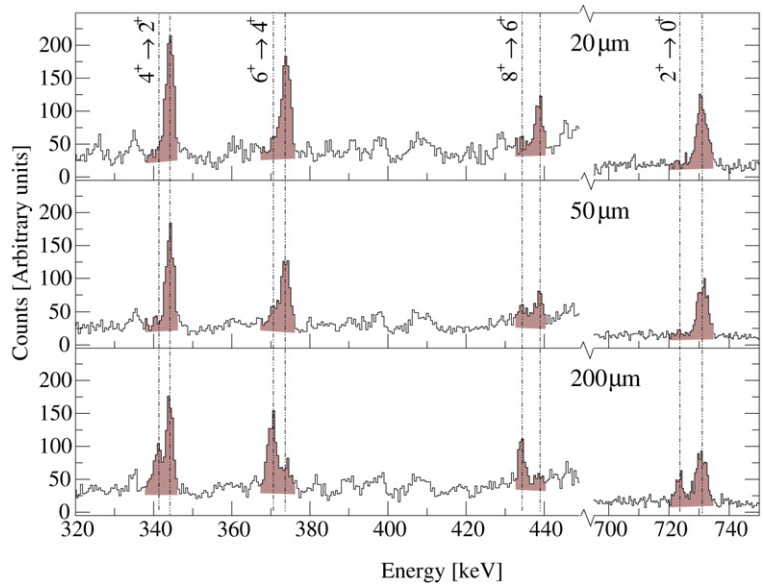

Fig. 3. Singles recoil-gated γ-ray spectra of ^{188}Pb measured at three target-to-degrader distances with five JUROGAM detectors at 158°. Lines indicate the positions of the fully Doppler-shifted and degraded components of the γ rays from the 2^+, 4^+, 6^+ and 8^+ yrast states. Relevant peak areas are shaded to guide the eye.

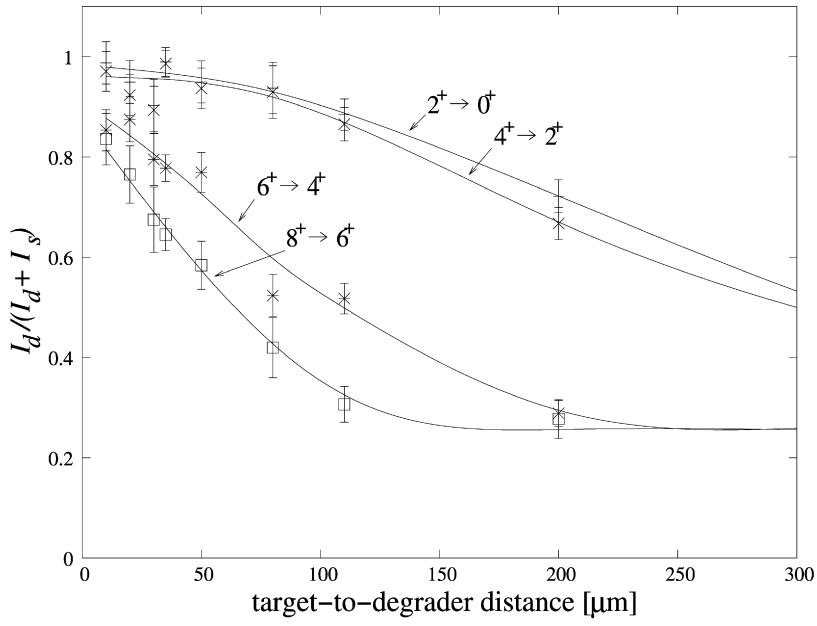

Fig. 4. Decay curves of four lowest yrast states in ^{188}Pb extracted from γ-ray spectra recorded with five JUROGAM detectors at 158°. The smooth lines are drawn to guide the eye.

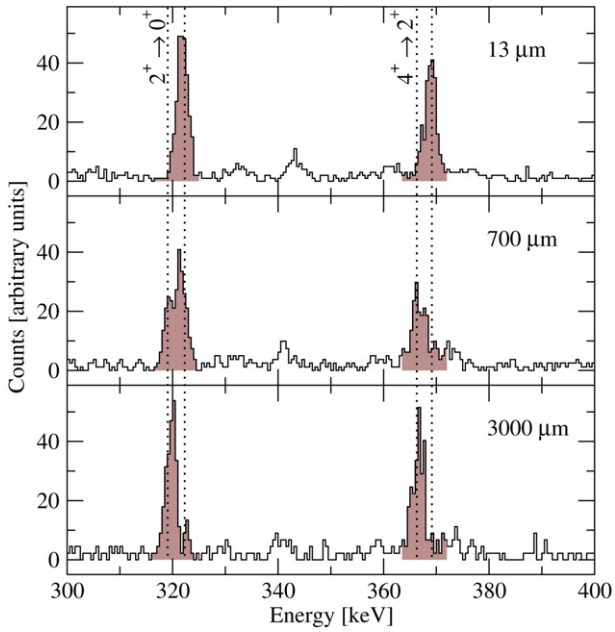

Fig. 5. Singles RDT γ-ray spectra of ^{194}Po measured at three target-to-degrader distances with five JUROGAM detectors at 158°. Lines indicate the positions of the fully Doppler-shifted and degraded components of the γ rays from the 2^+ and 4^+ yrast states. Relevant peak areas are shaded to guide the eye.

2.4. ^{194}Po

The ^{194}Po α decay with $t_{1/2} = 390$ ms and $E_\alpha = 6.99$ MeV was used to tag the prompt γ rays of interest to obtain singles RDT γ-ray spectra for 13 target-to-degrader distances, ranging from 5 μm to 3000 μm. The fusion–evaporation reaction ^{114}Cd(^{83}Kr, $3n$)^{194}Po with a beam energy of 375 MeV was used to populate excited states in ^{194}Po. The reaction cross section was approximately 120 μb, the lowest for an RDDS measurement. A stretched 1.0 mg/cm^2 Ta foil facing the beam was used to support a 1.0 mg/cm^2 ^{114}Cd target. With an initial recoil velocity of $v/c = 3.6\%$ a 1.0 mg/cm^2 Mg degrader foil was used to obtain the velocity of $v/c = 2.8\%$. Despite the limited statistics, the low background in the RDT γ-ray spectra still enabled the fully Doppler-shifted and degraded components of γ-rays from the 2^+ and 4^+ yrast states in ^{194}Po to be resolved. Sample γ-ray spectra are shown in Fig. 5 and decay curves extracted from the spectra are shown in Fig. 6. Experimental mean lifetimes τ extracted from the decay curves are listed in Table 1.

3. Results

Within the rotational model, quadrupole moments and deformation parameters can be extracted from the measured B(E2) values. Assuming a rotating, axially symmetric quadrupole deformed nucleus, the transition quadrupole moment Q_t can be extracted from the B(E2) values by using the formula

$$B(\mathrm{E2}; I \rightarrow I-2) = \frac{5}{16\pi} Q_t^2 \langle I020|I-20\rangle^2 \tag{1}$$

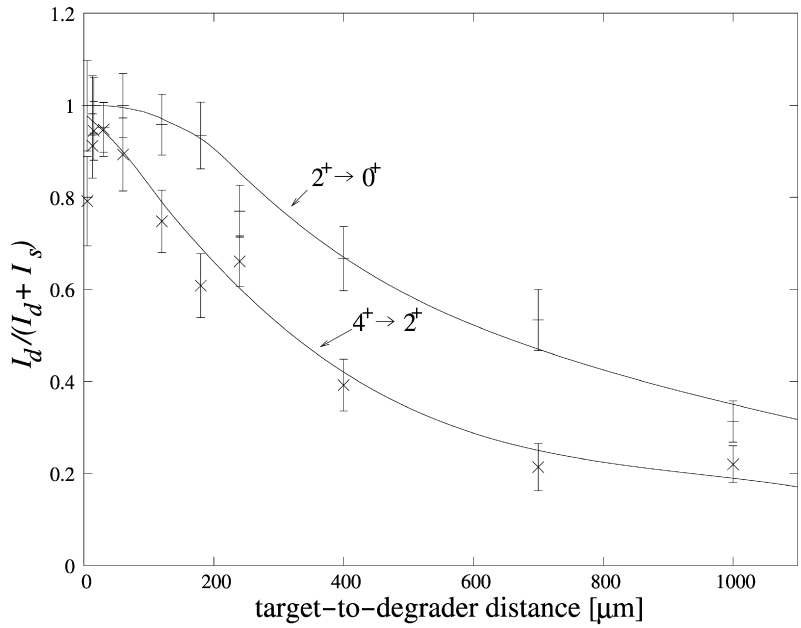

Fig. 6. Decay curves of two lowest yrast states in ^{194}Po extracted from γ-ray spectra recorded with ten JUROGAM detectors at 134°. The smooth lines are drawn to guide the eye.

Table 1
Electromagnetic properties of low-lying yrast states in ^{186,188}Pb and ^{194}Po extracted from the present lifetime measurements. In addition, the observed intensity balance $J_{\text{feed}}/J_{\text{depop}}$ is given. Transition energies E_γ are taken from Refs. [13, 14,16]

	E_γ [keV]	I_i^π	τ [ps]	B(E2) [W.u.]	$\lvert Q_t \rvert$ [eb]	$\lvert\beta_2^{(t)}\rvert$	$J_{\text{feed}}/J_{\text{depop}}$
^{186}Pb	662.2	2^+	18(5)	6(2)	1.3(2)	0.046(7)	0.95(9)
	260.6	4^+	18(4)	510(120)	10.3(10)	0.35(4)	0.78(9)
	337.1	6^+	6(2)	460(160)	10(2)	0.33(6)	0.80(10)
	414.8	8^+	5(2)	200(140)	6(2)	0.21(7)	0.57(5)
^{188}Pb	723.5	2^+	5–12	12–5	2.0–1.3	0.07–0.04	0.82(3)
	340.2	4^+	15.9(10)	160(10)	6.0(2)	0.205(7)	0.94(3)
	369.7	6^+	4.0(6)	440(70)	9.4(7)	0.32(3)	0.67(3)
	433.8	8^+	2.4(4)	350(60)	8.2(7)	0.28(3)	0.53(3)
^{194}Po	319.7	2^+	37(7)	90(20)	5.5(6)	0.18(2)	0.78(6)
	366.5	4^+	14(4)	120(40)	5.4(8)	0.17(3)	0.60(6)

assuming $K = 0$. For a perfect rotor $Q_t = Q_0$, the intrinsic quadrupole moment of the rotating nucleus. With the assumption of uniform charge distribution, the quadrupole deformation parameter β_2 is, in turn, linked to Q_0 by the formula

$$Q_0 = \frac{3}{\sqrt{5\pi}} ZeR_0^2\beta_2, \tag{2}$$

where $R_0 = 1.2A^{1/3}$ fm. This relation provides a simple rescaling of the quadrupole deformation and removes a trivial dependence on the number of protons. In the present work a notation of

$\beta_2^{(t)}$ for β_2 has been used in order to emphasise the fact that it is extracted from the experimental value of Q_t. Table 1 lists the results of the present work including B(E2) values, the absolute values of transition quadrupole moments and deformation parameters extracted for each of the measured E2 transition. In addition, the intensity balance $J_{\text{feed}}/J_{\text{depop}}$ describing the unobserved feeding is also given for each level of interest.

Up to 80% of the population intensity of the 2^+ yrast state in ^{188}Pb occurs via the 4^+ yrast state which has a relatively long lifetime (see decay curves in Fig. 4). This is due to the low transition energy of the $4^+ \rightarrow 2^+$ transition and the difference in the underlying nuclear structure of the 2^+ and 4^+ states. Therefore, the resulting value for the lifetime of the 2^+ state varies between 5 ps and 12 ps corresponding to unobserved feeding lifetimes of 16 ps and 0.1 ps, respectively. In Ref. [22] a value of 13(7) ps for the lifetime of the 2^+ state was obtained using coincidence measurements. This value would slightly favour the upper limit obtained in the present work. In the same work [22] $\tau = 16(8)$ ps for the 4^+ state in ^{188}Pb is obtained, which is in agreement with $\tau = 15.9(10)$ ps measured in the present work for this level. For all the other states measured in this work, the unobserved feeding assumption discussed in Section 2.1 is valid.

4. Discussion

4.1. Prolate yrast bands in ^{186}Pb and ^{188}Pb

The large absolute E2 transition probabilities of the $8^+ \rightarrow 6^+$ and $6^+ \rightarrow 4^+$ transitions in ^{186}Pb and ^{188}Pb reveal high collectivity of the yrast 4^+, 6^+ and 8^+ states in these nuclei and are in agreement with the hypothesis of prolate yrast states. A similar high E2 transition probability is observed for the $4^+ \rightarrow 2^+$ transition in ^{186}Pb indicating that the 2^+ state in ^{186}Pb is also a rather pure member of the prolate band. However, in ^{188}Pb the $4^+ \rightarrow 2^+$ transition rate is significantly lower than that in ^{186}Pb suggesting a strong admixture of other structures in the first excited 2^+ state of ^{188}Pb. The present results indicate that the ground states of even-mass Pb isotopes near the $N = 104$ mid shell have a structure significantly different from the low lying yrast states. The wave functions should be dominated by the spherical component, with small admixtures of deformed configurations. This is in agreement with recent isotope shift measurements providing mean square charge radii for neutron-deficient Pb isotopes [38].

If the intrinsic structure within the rotational band does not change and the system receives collectivity via pure rotation, the quadrupole moment within the band should be constant. The $|Q_t|$ values of Table 1 are plotted in Fig. 7 together with the kinematic moments of inertia $\mathcal{J}^{(1)}$ deduced from the measured level energies [13,14,16]. The strongly mixed character of the 2^+ state in ^{188}Pb is reflected as a $|Q_t|$ value for the 4^+ state significantly lower than that for the higher spin states. The same effect can also be seen in the kinematic moment of inertia $\mathcal{J}^{(1)}$ deduced from the energy of the $4^+ \rightarrow 2^+$ transition in ^{188}Pb. The maximum $|Q_t|$ value is reached already for the $4^+ \rightarrow 2^+$ transition in ^{186}Pb whereas in ^{188}Pb only at the $6^+ \rightarrow 4^+$ transition. In ^{186}Pb the $|Q_t|$ value for the 8^+ state seems to be significantly lower than for the 6^+ state suggesting a possible drop of collectivity. However, one should note that within the error bars, the $|Q_t|$ values for the 4^+, 6^+ and 8^+ states are all consistent with the constant $|Q_t|$ value within the rotational band. In particular, there is no anomaly in the kinematic moments of inertia, which would accompany a change of collectivity for the 8^+ state. Based on these observations the deformation for the prolate structure in light Pb isotopes can be deduced as an average of the $|\beta_2|$ values of the prolate 4^+, 6^+ and 8^+ states in ^{186}Pb and 6^+ and 8^+ states in ^{188}Pb, being

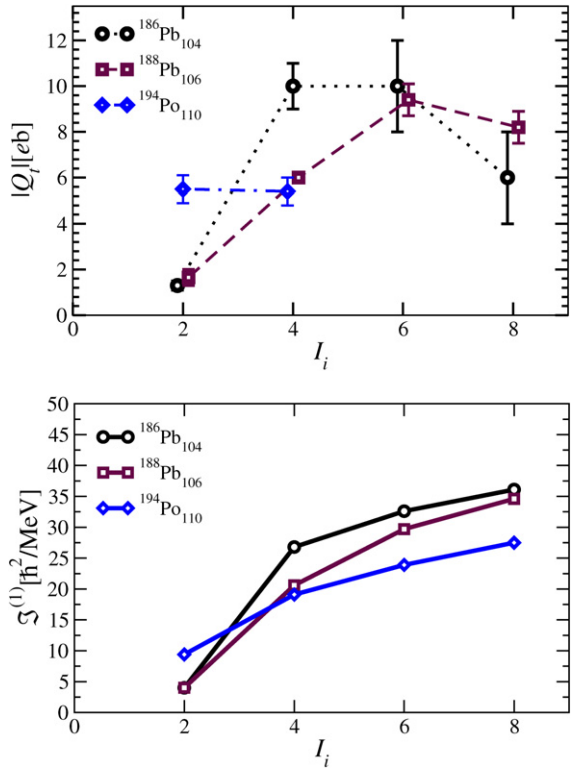

Fig. 7. Measured $|Q_t|$ values (upper panel) and the kinematic moments of inertia (lower panel) for ^{186}Pb, ^{188}Pb and ^{194}Po. Some of the $|Q_t|$ values are slightly displaced from their actual I_i value to maintain the clarity of presentation.

$|\beta_2| = 0.29(5)$. This value is in agreement with the theoretical values obtained using different approaches [6,7,39,40].

The excitation spectra and transition probabilities of even-mass neutron-deficient Pb isotopes have been calculated in Refs. [7,8] by mixing angular-momentum projected mean-field states corresponding to different intrinsic axial quadrupole deformations. More explanations on the general ideas of the model can be found in [41,42]. In those calculations, the same effective interaction determines the self-consistent mean-field states and the subsequent configuration mixing. In Ref. [7], the local Skyrme interaction SLy6 was used, while the authors of Ref. [8] employed the finite-range Gogny force D1S. In this mass region, a typical calculation mixes a set of projected states obtained from about 25 different intrinsic deformations, ranging from oblate to prolate deformation, covering several coexisting minima and the regions in between and around.

The method allows the fluctuations of the collective states around the various minima and their mixing to be deduced, which both calculations predict to be quite substantial for low-spin states in this mass region. The framework allows the B(E2) values between the mixed states to be calculated directly, which can in most cases be easily grouped into rotational bands (or vibrational structures) according to their B(E2) values and the strongest constituent of intrinsic states. In particular, the calculated in-band B(E2) values do not rely on the assumptions of the collective model. As the calculations use the full model space of occupied single-particle levels and the method does not contain a summation over unoccupied states, the bare charges are employed to

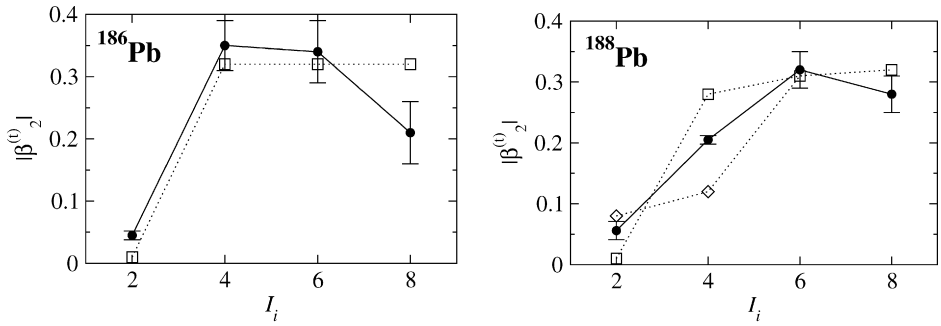

Fig. 8. A comparison of calculated (open symbols) [7,41] and measured (filled circles) quadrupole deformation parameters $|\beta_2^{(t)}|$ in ^{188}Pb and ^{186}Pb. For more details, see text.

calculate the B(E2) values. The corresponding more intuitive dimensionless transitional deformation parameters $\beta_2^{(t)}$ can be deduced from the calculated B(E2) values in the same manner as the experimental ones through Eqs. (1) and (2).

The calculations of Refs. [7,8] agree in their predictions for the overall features of ^{186}Pb and ^{188}Pb: the 0^+ ground state is predominantly spherical, with the tail of the wave function spreading to prolate and oblate shapes, while there are two coexisting low-lying rotational bands. For spins above 4^+ the states in these bands correspond to rather pure prolate or oblate configurations (meaning that the collective wave functions correspond to a wave packet localised in the respective potential well), with the prolate ones being yrast. In ^{186}Pb, both low-lying 2^+ states are predicted to be nearly pure prolate or oblate states as well, while in ^{188}Pb they are substantially mixed. The lowest 2^+ state remains predominantly prolate using the Gogny force D1S, while it is even pushed over to the oblate side using the Skyrme interaction SLy6.

The $|\beta_2^{(t)}|$ values for the yrast states taken from Ref. [7], together with the present experimental $|\beta_2^{(t)}|$ values for the yrast band are plotted in Fig. 8 for ^{186}Pb and ^{188}Pb. For ^{188}Pb, the additional $|\beta_2^{(t)}|$ values for the transitions to and from the predominantly oblate 2^+ state are shown. The calculated values reflect the features of the bands outlined above.

In ^{186}Pb, the prolate band does not mix substantially with other bands and the $|\beta_2^{(t)}|$ values are consistent with a constant value down to that for the transition from the 4^+ state to the 2^+ state. The drop for the 2^+ to ground state transition is then caused by the change to the predominantly spherical 0^+ ground state that only has a small contribution from prolate states. The calculation reproduces the data very well, noting that within error bars the experimental $|\beta_2^{(t)}|$ values are compatible with a constant value. The slight enhancement of the experimental $|\beta_2^{(t)}|$ for the 2^+ state decay suggests that either the 2^+ state should be more mixed with other structures, or, more probably, the 0^+ ground state should be spread more to prolate states.

In ^{188}Pb, the experimental $|\beta_2^{(t)}|$ value drops already for the transition from the 4^+ state to the 2^+ state. Two calculated $|\beta_2^{(t)}|$ values for this transition are given: that for the in-band transition to the predominantly prolate 2^+ state (open squares in Fig. 8), which is of about the same size than those for in-band transitions at higher spin; and the $|\beta_2^{(t)}|$ for the transition to the yrast 2^+ state, that has a strong oblate component (open diamonds in Fig. 8). The $|\beta_2^{(t)}|$ value for the former transition is significantly larger than the experimental one, while that for the latter transition much smaller. This suggests that the structure of the yrast 2^+ state should be in between those

Table 2
The B(E2) values in ^{186}Pb obtained in this work and with two theoretical approaches in Ref. [43]. The values are given in W.u.

I_i^π	This work	Mean-field	IBM
2^+	6(2)	1.6	8
4^+	510(120)	398	294
6^+	460(160)	480	403
8^+	200(140)	542	433

of the two calculated states. A very small relative shift in energy of a few hundred keV between the prolate and oblate minima could bring this modification. The precision of the method used in Refs. [7,8], that has no free parameters adjustable to the calculated nuclei, is not sufficient to account for such very fine details. Adding additional degrees of freedom to the method, in particular the explicit treatment of triaxiality, could also modify the wave function of strongly mixed states.

A very different approach to the mean-field calculations, the Interacting Boson Model (IBM), has also been used to describe the transition probabilities in ^{188}Pb [23]. These calculations reproduce the experimental B(E2) values for the $2^+ \rightarrow 0^+$ and $4^+ \rightarrow 2^+$ transitions relatively well, being 3 W.u. and 152 W.u. respectively (cf. 5–12 W.u. and 160(10) W.u. measured in this work). However, the collectivity of the assumed pure 6^+ and 8^+ prolate states is underestimated ($B(\mathrm{E2}; 6^+ \rightarrow 4^+) = 197$ W.u. and $B(\mathrm{E2}; 8^+ \rightarrow 6^+) = 215$ W.u.) in comparison to the experimental ones ($B(\mathrm{E2}; 6^+ \rightarrow 4^+) = 440(70)$ W.u. and $B(\mathrm{E2}; 8^+ \rightarrow 6^+) = 360(60)$ W.u.).

In Ref. [43] two different theoretical approaches have been used to describe the transition probabilities and level energies in ^{186}Pb. In addition to the aforementioned mean-field method, a different truncated shell-model approach has been taken, where multi-quasiparticle excitations across the $Z = 82$ shell gap give rise to configuration-mixed IBM states. The B(E2) values obtained with both of these approaches have been tabulated in Table 2. Theoretical values, resulting from both mean-field and shell-model calculations, reproduce the experimental values rather well, reaching the high level of collectivity already at the 2^+ yrast state.

4.2. Oblate yrast band in ^{194}Po

The present results reveal that the collectivity of the $2^+ \rightarrow 0^+$ and $4^+ \rightarrow 2^+$ transitions in ^{194}Po is much lower than that for the transitions between the prolate states in ^{186}Pb and ^{188}Pb. For the oblate structure the transition quadrupole moments are generally expected to be lower than those for the prolate structure. This weaker collectivity is also reflected in the smaller values of the kinematic moments of inertia for oblate states (see Fig. 7). The similar $|Q_t|$ values extracted from the $2^+ \rightarrow 0^+$ and $4^+ \rightarrow 2^+$ transitions in ^{194}Po (see Fig. 7) indicate a similar intrinsic structure of these lowest states. Consequently, also the ground state resembles predominantly the oblate shape. This is in contrast to the earlier conclusion in Ref. [16], where the ground state of ^{194}Po was deduced to be ∼50% of oblate character. The theoretical predictions of Refs. [5,44] indicate that the spherical configuration does not correspond to an energy minimum in even-mass Po isotopes and will not play the same role as in the Pb isotopes. Therefore, the effect of weak mixing of oblate and near spherical structures may well fit within the error bars of the measured transition probabilities. The dominance of oblate deformation in the ground state of ^{194}Po was predicted in Ref. [44], where a configuration mixing method similar to that of Ref. [7], but without projection on angular momentum was applied for neutron-deficient Po nuclei.

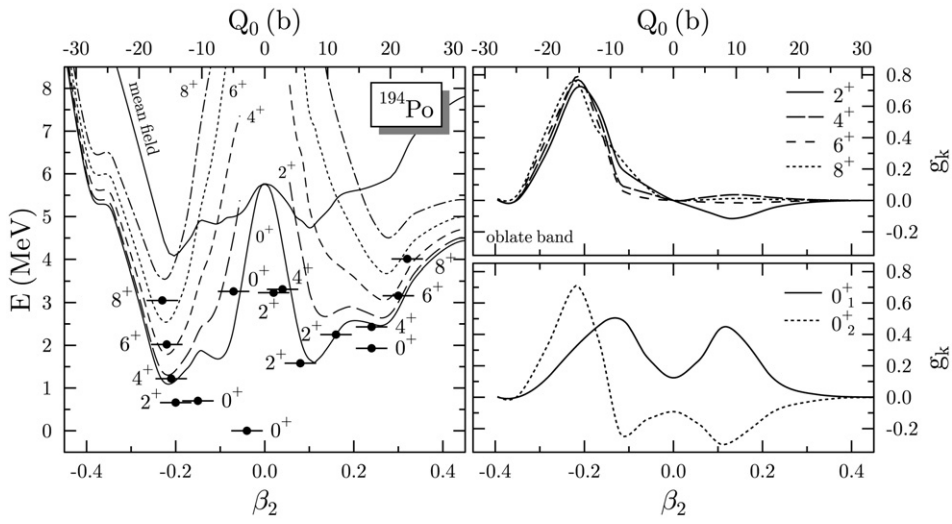

Fig. 9. Left panel: mean-field and angular-momentum projected deformation energy curves for $J = 0$–8 as a function of the intrinsic deformation β_2 of the mean-field states, together with selected collective states (see text) plotted at the average intrinsic deformation of the states they are constructed from. The energy scale is normalised to the 0^+ ground state obtained after configuration mixing. The upper scale shows the mass quadrupole moment of the intrinsic states. Lower right panel: collective wave functions g_k of the two lowest 0^+ states. Upper right panel: collective wave functions g_k of the 2^+–8^+ states in the oblate band. The same method and interaction as in Ref. [7] is used for the calculation.

Calculations in the frameworks of the Particle Core Model and the Quasiparticle Random Phase Approximation based on the multiphonon excitations have been carried out for ^{194}Po in Refs. [45,51]. However, these calculations fail to reproduce the experimental $B(\mathrm{E2})$ values, being approximately an order of magnitude too small. In these calculations the effect of particle–hole intruder structures is not taken into account. The failure to reproduce the measured $B(\mathrm{E2})$ values indicates the important role of intruder structures in enhancing the quadrupole collectivity in ^{194}Po. Recently, a study of α decays to the coexisting 0^+ states in neutron-deficient Po and Pb isotopes has been carried out within the framework of density dependent cluster model [46]. The magnitude of the nuclear deformation has been extracted from the experimental α decay energies and half-lives. The ground state of ^{194}Po was found to have deformed character, which agrees well with the dominating intruder component of the ground state deduced from the measured lifetimes.

In the present work, the excitation spectra and transition moments of low-lying collective states in ^{194}Po have been calculated using the same angular-momentum projected configuration-mixing method as in Ref. [7], employing the Skyrme interaction SLy6 in connection with a density dependent pairing interaction. Results relevant for the present discussion are shown in Fig. 9 in the same manner as in Ref. [7]. The calculated deformation energy curve of ^{194}Po shows an even richer topography than those of neutron-deficient Pb isotopes, with several competing minima or shoulders at small prolate and oblate deformations. An oblate minimum at $\beta_2 = -0.19$ provides the mean-field ground state. After projection on $J = 0$, the same minimum gives also the projected ground state, shifted to slightly larger oblate deformation. At small deformation, $|\beta_2| < 0.2$, the topography of the projected deformation energy curves changes rapidly with spin up to $J = 6$.

After configuration mixing, there are three coexisting low-lying collective structures at small deformation. The calculated ground-state wave function is nearly equally distributed around the spherical point at small prolate and oblate deformation, with a slight enhancement on the oblate side. An excited 2^+ state at about 1.6 MeV and a triplet of near-degenerate 0^+, 2^+ and 4^+ states at about 3.2 MeV, all with small average deformation, suggest a vibrational structure built on the ground state. There is also a low-lying oblate band, which is yrast at low spins. Its 0^+ band head and the ground state are strongly mixed, such that the 0^+_2 level is pushed above the 2^+ level in the oblate band. With increasing spin, the mixing of the states in this band with those in the other collective structures becomes rapidly suppressed, while their intrinsic deformation slowly moves towards larger deformation, which can be inferred from both the collective wave functions g_k and the average intrinsic deformation of these states. Both findings are similar to what has been found in similar calculations for Pb isotopes [7]. One should note, however, that the square of $g_k(\beta_2)$ does not give the probability of finding a projected mean-field state of intrinsic deformation β_2 in the mixed wave function, as projected mean-field states (of same spin) do not form an orthogonal basis. At higher excitation energy, the present calculation also gives a prolate band which never becomes yrast, as at even larger prolate deformations beyond those shown in Fig. 9 the calculation additionally predicts two low-lying superdeformed structures. One of the corresponding bands becomes yrast at spin 6^+, which is expected to be much too low as the excitation energies of the band heads of the known superdeformed bands in the adjacent Pb isotopes are underestimated by 1 MeV by the same effective interaction [7].

The calculated density of excited levels, both vibrational and rotational, is expected to be too dilute as in all earlier calculations using similar methods [7,8]. This is a well-known deficiency of the so-called "Peierls–Yoccoz" moments of inertia that correspond to this method, which is in turn related to the symmetries imposed on the mean-field states in the present calculation. These exclude certain time-reversal breaking mean fields that after projection will lower the excitation energies, but usually leave the deformation of the bands nearly untouched.

The 4^+ and 2^+ levels corresponding to the two observed γ transitions are predicted to be oblate, as one can see in Fig. 9. The Q_t values that are obtained for the transitions between the yrast states are $Q_t(4^+_{\rm obl} \rightarrow Q_t 2^+_{\rm obl}) = 6.4$ eb and $Q_t(2^+_{\rm obl} \rightarrow 0^+_{\rm gs}) = 3.7$ eb, and correspond to $\beta_2^{(t)}(4^+) = 0.21$ and $\beta_2^{(t)}(2^+) = 0.12$. In the calculation, the lower value of $\beta_2^{(t)}$ obtained for the 2^+ state is due to a combination of two factors: the decrease of the intrinsic deformation when going down in the band, and the structure of the 0^+ ground state wave function which has nearly equal oblate and prolate components. This decrease does not agree with the experimental results, the two observed Q_t values being equal. Since the calculated $Q_t(4^+)$ is close to the observed one, the too small value obtained for the $Q_t(2^+)$ value can probably be traced back to a deficiency in the description of the 0^+ ground state. Indeed, the transition quadrupole moment for the (energetically forbidden) transition from the oblate 2^+ state to the second 0^+ is $Q_t(2^+) = 5.2$ eb which corresponds to $\beta_2^{(t)} = 0.169$, much closer to the experimental value. One can infer from this result that the mean-field oblate minimum should be slightly lower in energy, in such way that the oblate component of the ground state wave function will be larger. This hypothesis is consistent with the findings of Ref. [7] on the adjacent Pb isotopes, where the oblate band heads are always slightly too high in excitation energy. Still, the calculation correctly predicts that the oblate states are lowered when going from the Pb to the Po isotone.

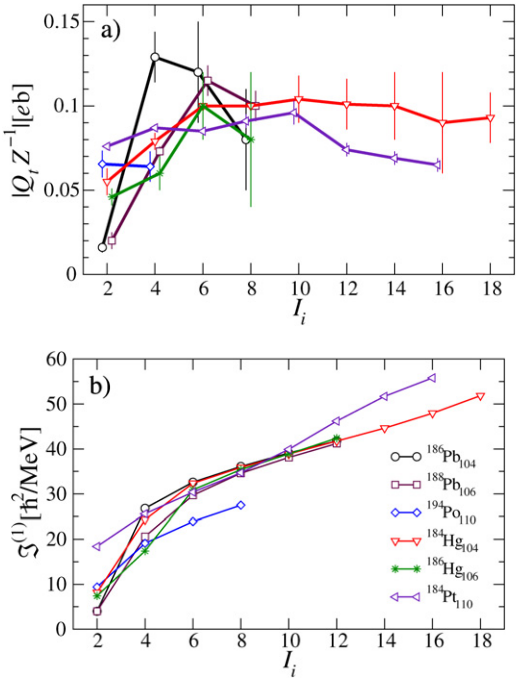

Fig. 10. Values of $|Q_t Z^{-1}|$ (a) extracted from lifetime measurements together with (b) the corresponding values of kinematic moments of inertia for a selection of nuclei in the vicinity of neutron-deficient Pb nuclei. The lifetime data from Refs. [47–49] and from the present work are used. Some of the $|Q_t Z^{-1}|$ data points are slightly displaced from their actual I_i value to maintain the clarity of presentation.

4.3. Collectivity in neutron mid-shell nuclei near $Z = 82$

Prolate yrast bands with kinematic moments of inertia very similar to the prolate bands of ^{186}Pb and ^{188}Pb have been observed in even-mass Hg and Pt nuclei near the $N = 104$ mid-shell (Fig. 10(b)). Lifetime measurements of yrast levels have been carried out for ^{184}Hg [47], ^{186}Hg [48], and ^{184}Pt [49]. Since the quadrupole moment is charge dependent, a parameter $|Q_t Z^{-1}|$ is chosen to compare experimental quadrupole moments of nuclei with different Z. In Fig. 10(a), a selection of $|Q_t Z^{-1}|$ values extracted from the aforementioned measurements are shown together with the present results for ^{186,188}Pb and ^{194}Po.

The ground state and the lowest 2^+ state in ^{184}Hg and in ^{186}Hg are assumed to represent a weakly deformed oblate shape [47] with a $\pi(0p\text{–}2h)$ configuration [50]. The extracted $|Q_t Z^{-1}| \approx 0.05$ eb for those states indicates that collectivity of the $\pi(0p\text{–}2h)$ configuration is lower than that for the $\pi(4p\text{–}2h)$ configuration in ^{194}Po ($|Q_t Z^{-1}| \approx 0.065$). At higher spin the yrast line in ^{184}Hg and in ^{186}Hg is formed by the more deformed prolate ($|Q_t Z^{-1}| \approx 0.10$ eb) structure similar to that in the Pb isotones.

In ^{184}Pt the ground-state band has been assigned as a prolate deformed intruder band with a $\pi(6p\text{–}2h)$ configuration. This structure belongs to the same intruder spin multiplet as the prolate $\pi(4p\text{–}4h)$ states in ^{188}Pb [50] and therefore, should generate similar band structures. In Ref. [49], the deviation of the measured $B(E2)$ values for the low-spin yrast states in ^{184}Pt from those for an ideal rotor, is deduced to be due to a mixture of weakly deformed structures.

As seen in Fig. 10(b) the kinematic moments of inertia for the $8^+ \rightarrow 6^+$ and $6^+ \rightarrow 4^+$ transitions are very similar for ^{184}Hg, ^{184}Pt and ^{186,188}Pb. The corresponding $|Q_t Z^{-1}|$ values extracted from the measured lifetimes may indicate slightly decreasing collectivity with decreasing proton number. However, more precise measurements are needed to confirm this conclusion.

5. Summary

RDDS lifetime measurements of yrast states in ^{186,188}Pb and ^{194}Po have been carried out. The Köln plunger device was installed at the JUROGAM target position and coupled to the RITU gas-filled separator. Evaporation residues were separated from scattered beam and fission products and identified by the GREAT spectrometer at the focal plane of RITU. As these pioneering experiments demonstrate, the RDT technique provides essentially background free γ-ray spectra for lifetime measurements and enables the extension of the RDDS studies to exotic nuclei near the proton drip line produced with relatively low cross sections.

Reduced transition probabilities B(E2), derived from the measured lifetimes confirm the high collectivity of the intruder states in this region. Values for the quadrupole deformation parameter $|\beta_2| = 0.29(5)$ (^{186,188}Pb) and $|\beta_2| = 0.17(3)$ (^{194}Po) were extracted for the prolate and oblate bands, respectively.

The observed relatively low collectivity for the $4^+ \rightarrow 2^+$ transition in ^{188}Pb indicates that the mixing of the oblate and prolate shapes still plays a crucial role in the lowest energy 2^+ state of this Pb isotope. In contrast, the high collectivity of the corresponding transition in ^{186}Pb reveals that this yrast 2^+ state in ^{186}Pb is already a pure member of the prolate band.

A comparison of the present results for ^{186,188}Pb with the earlier lifetime measurements of prolate states in ^{184,186}Hg and ^{184}Pt indicates similarities between the corresponding bands, as would be expected on the basis of similar kinematic moments of inertia.

In ^{194}Po, on the basis of observed and calculated quadrupole moments, the oblate component could dominate the ground state. This is also suggested by the results of self-consistent mean-field calculations carried out in the present work, which provide theoretical Q_t values for the transitions under investigation. To study the collectivity in neutron-deficient Po nuclei further, lifetime measurements of the heavier Po isotopes, where the intruder structures lie higher in energy, are required.

Acknowledgements

This work has been supported by the Academy of Finland (the Finnish Centre of Excellence Programme, project 44875), the EU-FP5 projects EXOTAG (HPRI-1999-CT-50017) and Access to Research Infrastructure (HPRI-CT-1999-00044), the BMBF (Germany) under contract No. 06K167, European Community Marie Curie Fellowship, the Belgian Science Policy office under contract PAI P5-07 and the US D.O.E. under grant No. DE-FG02-91ER-40609. The UK/France (EPSRC/IN2P3) Loan Pool and GAMMAPOOL network are acknowledged for the EUROGAM detectors of JUROGAM.

References

[1] J.L. Wood, et al., Phys. Rep. 215 (1992) 101.
[2] R. Julin, K. Helariutta, M. Muikku, J. Phys. G 27 (2001) R109.
[3] A.N. Andreyev, et al., Nature (London) 405 (2000) 430.
[4] C. De Coster, B. Decroix, K. Heyde, Phys. Rev. C 61 (2000) 067306.

[5] F.R. May, V.V. Paskevich, S. Frauendorf, Phys. Lett. B 68 (1977) 113.
[6] W. Nazarewicz, Phys. Lett. B 305 (1993) 195.
[7] M. Bender, P. Bonche, T. Duguet, P.-H. Heenen, Phys. Rev. C 69 (2004) 064303.
[8] R.R. Rodríguez-Guzmán, J.L. Egido, L.M. Robledo, Phys. Rev. C 69 (2004) 054319.
[9] D.G. Jenkins, et al., Phys. Rev. C 62 (2000) 021302(R).
[10] J.F.C. Cocks, et al., Eur. Phys. J. A 3 (1998) 17.
[11] A.M. Baxter, et al., Phys. Rev. C 48 (1993) R2140.
[12] J. Heese, et al., Phys. Lett. B 302 (1993) 390.
[13] J. Pakarinen, et al., Phys. Rev. C 72 (2005) 011304(R).
[14] G.D. Dracoulis, et al., Phys. Rev. C 69 (2004) 054318.
[15] N. Bijnens, et al., Phys. Rev. Lett. 75 (1995) 4571.
[16] K. Helariutta, et al., Eur. Phys. J. A 6 (1999) 289.
[17] L.A. Bernstein, et al., Phys. Rev. C 52 (1995) 621.
[18] W. Younes, et al., Phys. Rev. C 52 (1995) R1723.
[19] K. Van de Vel, et al., Eur. Phys. J. A 17 (2003) 167.
[20] K. Van de Vel, et al., Eur. Phys. J. A 24 (2005) 57.
[21] A.N. Andreyev, et al., Phys. Rev. C 73 (2006) 044324.
[22] A. Dewald, et al., Phys. Rev. C 68 (2003) 034314.
[23] V. Hellemans, et al., Phys. Rev. C 71 (2005) 034308.
[24] R.G. Allatt, et al., Phys. Lett. B 437 (1998) 29.
[25] A.N. Andreyev, et al., J. Phys. G 25 (1999) 835.
[26] A.M. Oros, et al., Nucl. Phys. A 645 (1999) 107.
[27] E.S. Paul, et al., Phys. Rev. C 51 (1995) 78.
[28] T. Grahn, et al., Phys. Rev. Lett. 97 (2006) 062501.
[29] C.W. Beausang, et al., Nucl. Instrum. Methods A 313 (1992) 37.
[30] M. Leino, et al., Nucl. Instrum. Methods B 99 (1995) 653.
[31] R.D. Page, et al., Nucl. Instrum. Methods B 204 (2003) 634.
[32] I.H. Lazarus, et al., IEEE Trans. Nucl. Sci. 48 (2001) 567.
[33] P. Rahkila, arXiv: 0711.3364 [nucl-ex], Nucl. Instrum. Methods A, submitted for publication.
[34] A. Dewald, S. Harissopulos, P. von Brentano, Z. Phys. A 334 (1989) 163.
[35] P. Petkov, et al., Nucl. Phys. A 543 (1992) 589.
[36] S. Harissopulos, et al., Nucl. Phys. A 467 (1987) 528.
[37] P. Petkov, et al., Phys. Rev. C 62 (2000) 014314.
[38] H. De Witte, et al., Phys. Rev. Lett. 98 (2007) 112502.
[39] T. Nikšić, et al., Phys. Rev. C 65 (2002) 054320.
[40] J.L. Egido, L.M. Robledo, R.R. Rodríguez-Guzmán, Phys. Rev. Lett. 93 (2004) 082502.
[41] M. Bender, P.-H. Heenen, Eur. Phys J 25 (2005) 519.
[42] J.L. Egido, L.M. Robledo, in: G.A. Lalazissis, P. Ring, D. Vretenar (Eds.), Extended Density Functionals in Nuclear Physics, in: Lecture Notes in Physics, vol. 641, Springer, Berlin, 2004, p. 269.
[43] J. Pakarinen, et al., Phys. Rev. C 75 (2007) 014302.
[44] N.A. Smirnova, P.-H. Heenen, G. Neyens, Phys. Lett. B 569 (2003) 151.
[45] S. Peltonen, D.S. Delion, J. Suhonen, Phys. Rev. C 71 (2005) 044315.
[46] C. Xu, Z. Ren, Phys. Rev. C 75 (2007) 044301.
[47] W.C. Ma, et al., Phys. Lett. B 167 (1986) 277.
[48] D. Proetel, R.M. Diamond, F.S. Stephens, Phys. Lett. 48B (1974) 102.
[49] U. Garg, et al., Phys. Lett. B 180 (1986) 319.
[50] C. De Coster, et al., Nucl. Phys. A 621 (1997) 802.
[51] W. Younes, J.A. Cizewski, Phys. Rev. C 55 (1997) 1218.